

Momentum-space signatures of the Anderson transition in a symplectic, two-dimensional, disordered ultracold gas

Ehsan Arabahmadi ¹, Daniel Schumayer ^{1,*}, Benoît Grémaud ^{2,3,4},
Christian Miniatura ^{3,4,5,6,7} and David A. W. Hutchinson ^{1,4}

¹Dodd-Walls Centre for Photonic and Quantum Technologies, Department of Physics, University of Otago, Dunedin, New Zealand

²Aix Marseille Université, Université de Toulon, Centre National de la Recherche Scientifique, CPT, Marseille, France

³MajuLab, CNRS-UCA-SU-NUS-NTU International Joint Research Unit, Singapore

⁴Centre for Quantum Technologies, National University of Singapore, Singapore

⁵Department of Physics, National University of Singapore, Singapore

⁶School of Physical and Mathematical Sciences, Nanyang Technological University, Singapore

⁷Université Côte d'Azur, CNRS, Institut de Physique de Nice, Nice, France



(Received 16 January 2023; revised 11 August 2023; accepted 6 November 2023; published 25 January 2024)

We study Anderson localization in two-dimensional, disordered, spin-orbit systems belonging to the symplectic symmetry class using momentum-space signatures such as the coherent backscattering antipeak and the coherent forward-scattering peak. Significantly, these momentum-space features are readily accessible in ultracold atom experiments through absorption imaging after time-of-flight expansion. Here, the critical exponent and mobility edge of the metal-insulator transition are successfully obtained through a finite-time analysis of the coherent backscattering width. An anomalous residual diffusion, unique to two dimensions, is identified at the transition point where the system changes from a metal to an insulator. A spin localization phenomenon is also observed in the deep localized regime.

DOI: [10.1103/PhysRevResearch.6.L012021](https://doi.org/10.1103/PhysRevResearch.6.L012021)

Introduction. Anderson localization (AL), the disorder-induced suppression of wave transport by destructive interference, was first introduced [1] to explain the anomalous suppression of conductance in mesoscopic electron systems. It is, in fact, a general phenomenon, and an ubiquitous feature of any linear waves propagating in bulk random media. Since its conceptual inception, it has been observed (if indirectly) in a variety of very different systems [2–18]. Notably, over the past decade, ultracold atomic gases have provided a uniquely controllable experimental platform in which to directly observe and study AL in quantum systems [13,19–24].

In particular, the momentum distribution of the single-particle wave function has provided a directly observable signature of both weak localization and strong localization through the coherent backscattering (CBS) and coherent forward-scattering (CFS) peaks [28–32]. Their dynamic observation can be used to quantitatively characterize the three-dimensional (3D) Anderson transition delineating an extended metallic regime from an insulating one [31,32].

Historically, the first powerful phenomenological description of AL was the one-parameter scaling theory [33,34]. It relies on the hypothesis that all transport properties of a disor-

dered system depend only on the dimensionless conductance g . The scaling behavior of g with the system size L is encapsulated in the function $\beta(g) = \frac{d \ln g}{d \ln L}$ and obtained from a smooth interpolation between the limiting metallic and insulating expected asymptotics. This theory predicts the existence of a metal-insulator transition (MIT) in three dimensions [3,35]. It was also conjectured that there are distinct universality classes based on the symmetries of the Hamiltonian: orthogonal, unitary, and symplectic (see Table I). For example, ultracold atoms spreading in an optical speckle potential, where both time and spatial rotational symmetries are present, are well described by the Gaussian orthogonal ensemble (GOE) of random matrix theory [36]. It is also well known that disordered systems within this symmetry class are always localized for any disorder strength in dimension two or less, whereas they exhibit a metal-insulator transition in dimension three. In particular, both the mobility edge and critical exponent of this Anderson transition have been determined through the scaling behaviors of the CBS width and CFS contrast [31,32].

On the other hand, AL within the unitary and symplectic symmetry classes has received less experimental attention in the ultracold atom community [25–27,37]. Here we address the symplectic case by considering spin- $\frac{1}{2}$ particles in a two-dimensional (2D) square lattice with on-site disorder and random spin rotation during hopping. As is well known, spin-orbit coupling induces a MIT in two dimensions at low enough disorder [27,38]. We use the scaling properties of the CBS (anti)peak present in the momentum distribution of the particles to extract the mobility edge and critical exponent of this transition. The scaling behavior of the CFS peak contrast will be addressed in future work.

*daniel.schumayer@otago.ac.nz

Published by the American Physical Society under the terms of the [Creative Commons Attribution 4.0 International license](https://creativecommons.org/licenses/by/4.0/). Further distribution of this work must maintain attribution to the author(s) and the published article's title, journal citation, and DOI.

TABLE I. Phases in symmetry classes and dimensions. Abbreviations: metal-insulator transition (MIT); localized states (L). Corresponding review articles are Refs. [25–27].

| Symmetry | Dimensionality | | | | System |
|------------|----------------|-----|-----|-----|---|
| | 1 | 2 | 3 | >3 | |
| Orthogonal | L | L | MIT | MIT | No spin-orbit coupling, no magnetic field |
| Symplectic | L | MIT | MIT | MIT | Spin-orbit coupling |
| Unitary | L | L | MIT | MIT | Magnetic field |

Methods. Our tight-binding Hamiltonian for noninteracting spin- $\frac{1}{2}$ particles reads

$$H = J \sum_{\langle i, j \rangle} \psi_i^\dagger U_{ij} \psi_j + \sum_i w_i \psi_i^\dagger \psi_i, \quad (1)$$

where the sums run over all nearest-neighbor lattice site pairs $\langle i, j \rangle$ and lattice sites i , respectively. The field operator $\psi_i^\dagger = (\psi_{i\uparrow}^\dagger, \psi_{i\downarrow}^\dagger)$ is the two-component row-spinor built from the creation operators $\psi_{i\sigma}^\dagger$ at site i and spin components $\sigma = \uparrow$ and \downarrow . The on-site disorder potentials w_i are independent random variables uniformly distributed over $[-W/2, W/2]$, where W is the disorder strength. Hereafter, we set the hopping amplitude to $J = 1$ and the lattice spacing $a = 1$ and $\hbar = 1$. The random spin rotation during hopping is described by the $SU(2)$ matrix [37]

$$U_{ij} = \begin{bmatrix} e^{i\alpha_{ij}} \cos(\beta_{ij}) & e^{i\gamma_{ij}} \sin(\beta_{ij}) \\ -e^{-i\gamma_{ij}} \sin(\beta_{ij}) & e^{-i\alpha_{ij}} \cos(\beta_{ij}) \end{bmatrix}, \quad (2)$$

where the angles α_{ij} and γ_{ij} are independent random variables uniformly distributed over $[0, 2\pi)$, while the angles β_{ij} are independent random variables distributed over $[0, \pi/2]$ with probability density function $g(\beta) = \sin(2\beta)$. Since H is Hermitian, $U_{ij} = U_{ji}^\dagger$ implying $\alpha_{ij} = -\alpha_{ji}$ and similarly for γ_{ij} and β_{ij} .

One recovers the GOE case for $\beta_{ij} = 0$ and constant uniform angles α_{ij} and γ_{ij} . Noticeably, H is invariant under time reversal, $THT^{-1} = H$, where T is the time reversal operator for spin- $\frac{1}{2}$ systems and satisfying [39] $T^2 = -\mathbb{1}$. As a consequence, each eigenvalue ε_n of H is doubly degenerate (Kramers' degeneracy) with orthonormal eigenstates of the form $|\varphi_n\rangle$ and $|T\varphi_n\rangle$.

Importantly, the Hamiltonian dynamics cannot couple time-reversed states, irrespective of the disorder configuration. Indeed

$$\begin{aligned} \langle T\psi | e^{-iHt} | \psi \rangle &= \sum_n e^{-i\varepsilon_n t} [\langle T\psi | \varphi_n \rangle \langle \varphi_n | \psi \rangle \\ &\quad + \langle T\psi | T\varphi_n \rangle \langle T\varphi_n | \psi \rangle]. \end{aligned}$$

Using the $\langle T\psi | T\varphi_n \rangle = \langle \varphi_n | \psi \rangle$ relationship together with $\langle T\varphi_n | \psi \rangle = -\langle T\varphi_n | T^2\psi \rangle = -\langle T\psi | \varphi_n \rangle$, we see that the bracketed term in the sum above vanishes. As will be seen later, this very fact explains why a CBS dip, rather than a CBS peak, is observed in the momentum distribution for symplectic systems.

Results. To study the momentum-space signatures of AL, we consider the initial plane wave state $|\mathbf{k}_0, \uparrow\rangle$ at wave vector $\mathbf{k}_0 = (0, \pi/2)$ that we shape into a wave packet

$|\psi_0\rangle = \mathcal{F}(E, \delta E) |\mathbf{k}_0, \uparrow\rangle$ at energy E by the filter operator $\mathcal{F}(E, \delta E) \propto \exp[-(H - E)^2 / (2\delta E^2)]$. We then compute the disorder-averaged momentum distributions $n_\sigma(\mathbf{k}, t) = \overline{|\langle \mathbf{k}, \sigma | \exp(-iHt) |\psi_0\rangle|^2}$ at energy E ($\sigma = \uparrow, \downarrow$). The parameter δE that controls the selected energy window around E should be as narrow as possible to give a high resolution in energy and simultaneously wide enough to keep a sufficient number of eigenstates for averaging purposes. This filtering procedure [40] gives the momentum distribution at energy E for times $t \gg 1/(2\delta E)$. In all our numerical simulations, we have chosen $\delta E = 0.035$ (in units of J), allowing to study the momentum distribution at energy E for times $t \gtrsim 100$. In the rest of the paper, we have further chosen $E = 1$ (in units of J).

Figure 1 shows the momentum distributions obtained at time $t = 100$ (in units of \hbar/J) for on-site disorder strength $W = 6.8J$ (localized phase as will be seen later). In the spin-preserving channel, we observe a CFS peak centered at \mathbf{k}_0 on top of a flat diffusive background. In the spin-flipping channel, we observe a CBS antipeak centered at $-\mathbf{k}_0$ and dug into a flat background. Since $|\mathbf{k}_0, \downarrow\rangle = T|\mathbf{k}_0, \uparrow\rangle$, the dynamics cannot connect these two states and $n_\downarrow(-\mathbf{k}_0, t) = 0$ at any time, irrespective of the disorder configuration averaging. The CBS dip is thus a genuine characteristic of symplectic systems.

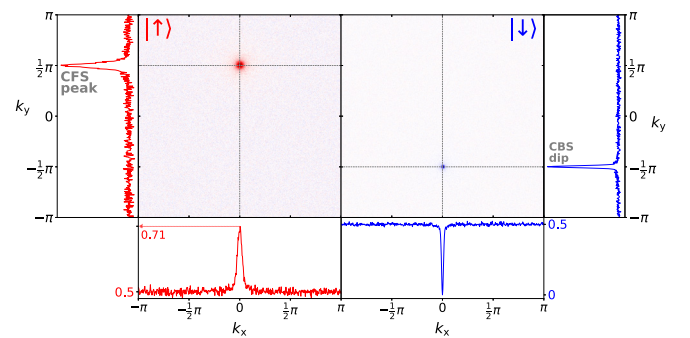


FIG. 1. Momentum distributions $n_\uparrow(\mathbf{k}, t)$ and $n_\downarrow(\mathbf{k}, t)$ obtained at time $t = 100\hbar/J$ for an initial state $|\mathbf{k}_0, \uparrow\rangle$ with $\mathbf{k}_0 = (0, \pi/2)$ filtered at energy $E = 1$ (in units of J). The linear size of the lattice is $L = 513$ (in units of a) and the on-site disorder strength is $W = 6.8$ (in units of J). The CFS peak and the CBS dip are clearly seen in their respective spin channels. At $t = 100\hbar/J$, the backgrounds in each spin channel have already reached their stationary and equal values (set to $\frac{1}{2}$ by total probability conservation). However, the CFS contrast has not yet reached the stationary value $C_F^\infty = 2$ expected for GSE systems.

In addition, we note that both backgrounds in each spin channel are flat. This can be traced back to the fact that the disorder-averaged Green's function $\overline{G(E)} = (E - H)^{-1}$, which is a diagonal operator in momentum and spin spaces as disorder average restores translation and rotation invariances, has diagonal elements that do not depend on \mathbf{k} and σ but only on E , i.e., $\langle \mathbf{k}, \sigma | \overline{G(E)} | \mathbf{k}, \sigma \rangle = \overline{g(E)}$. This unusual property, that we have checked numerically, can be explained by the fact that the disorder-averaged Hamiltonian vanishes ($\overline{H} = 0$), amounting to having a trivial \mathbf{k} -independent diagonal disorder-free Green's function $\langle \mathbf{k}'\sigma' | G_0(E) | \mathbf{k}\sigma \rangle = \delta_{\mathbf{k}\mathbf{k}'}\delta_{\sigma\sigma'}/(E + i0^+)$, and by the fact that the various correlators $\langle \mathbf{k}\sigma | \overline{H^n} | \mathbf{k}\sigma \rangle$, appearing in the Dyson series, are independent of \mathbf{k} for the uncorrelated hopping and on-site independent disorders that we consider here. A proof, for Gaussian disorder, can be found in the Appendix of [41]. This has to be contrasted with the standard situation of on-site disorder only where the disorder-averaged Hamiltonian exhibits a well-defined band structure $\epsilon_{\mathbf{k}}$ in momentum space. This entails \mathbf{k} -dependent diagonal elements of the free Green's function $\langle \mathbf{k}\sigma | G_0(E) | \mathbf{k}\sigma \rangle = (E - \epsilon_{\mathbf{k}} + i0^+)^{-1}$. Finally, from both diagrammatic approach and numerical computations, one can show that $\overline{g(E)} = [E - \Sigma(E)]^{-1}$, where the complex-valued scalar $\Sigma(E)$ is the self-energy. Therefore, one expects not only the backgrounds in each spin channel to be flat in the Brillouin zone, but also to grow with the same scattering time scale $\tau_s(E) = \hbar/[2|\text{Im}(\Sigma)|]$, before reaching the same stationary values.

Since $n_{\downarrow}(-\mathbf{k}_0, t) = 0$ at any time, the flat diffusive background in the \downarrow channel grows "around" the CBS dip. As time further increases, the CBS width shrinks and its temporal behavior depends on whether the system is diffusive, localized, or critical. The CFS peaks develop and grow in the \uparrow channel on a time scale given by the localization time τ_{loc} . It reaches a stationary peak-to-background relative contrast C_F^{∞} at "infinite" times, $t \gg \tau_{\text{loc}}$. Based on the statistical properties of the eigenfunctions in the GSE ensemble, we expect $C_F^{\infty} = 2$ instead of the $C_F^{\infty} = 1$ for GOE systems. Note that, in Fig. 1, the momentum distributions are plotted at a time where the CFS peak has not yet reached its stationary value. Note also that deviations from the GSE value are expected when the localization length becomes too small, and comparable to the lattice constant, at large W values [42,43]. On the other hand, by definition, the stationary CBS dip-to-background relative contrast is always $C_B^{\infty} = 1$, like in the GOE case. In the remainder of this Letter, we focus on the CBS dynamics.

a. CBS width dynamics. We define the CBS width Δk as the momentum size of the dip at half maximum of the diffusive background in the spin-flipping channel. In the metallic regime, the CBS antipeak continues to shrink in time and asymptotically tends to zero. At large enough times, its width is given by [40]

$$\Delta k(t) = \sqrt{\frac{\ln 2}{D(E, W)t}} \quad (\text{metallic phase}), \quad (3)$$

where $D(E, W)$ is the diffusion constant at energy E and disorder strength W . In the insulating regime, the CBS width decreases until it asymptotically approaches a constant value which defines the localization length at energy E and disorder

strength W

$$\Delta k(t \rightarrow +\infty) = \frac{1}{\xi_{\text{loc}}(E, W)} \quad (\text{insulating phase}). \quad (4)$$

At fixed energy, $\xi_{\text{loc}} \sim |W - W_c|^{-\nu}$ diverges algebraically with a critical exponent ν when approaching the critical point W_c . Thus ξ_{loc} quickly exceeds the maximum linear size L of the lattice that is computationally manageable and the system appears diffusive (in other words, Δk sticks to the mesh size $2\pi/L$ in momentum space). This is the reason why we resort to finite-time scaling methods [31,32,42,44–46] of Δk and introduce the length scale L_t through $t = 2\pi\rho(E)L_t^2$, where $\rho(E, W) = (1/L)^2 \sum_n \delta(E - \epsilon_n)$ is the disorder-averaged density of states (DOS) per unit surface of the system at energy E and disorder strength W .

b. Finite-time scaling. Following the single-parameter scaling rationale [34], we assume that there exists a single correlation length ξ subsuming all the microscopic details of the system. This correlation length identifies with the localization length in the insulating regime. As a consequence, the inverse of the rescaled CBS width is a continuous and smooth function of the single variable L_t/ξ that we recast under the form

$$\Lambda \equiv [\Delta k L_t]^{-1} = F(z), \quad (5)$$

where $z = \eta(E, W)L_t^{1/\nu}$, $\eta(E, W) = \xi^{-1/\nu}$, and $F(z)$ is a function characteristic of the transition. Working at fixed energy, we now Taylor expand $F(z)$ and $\eta(E, W)$ up to some expansion orders [32,47], $F(z) = \sum_{n=0}^N F_n z^n$ and $\eta(E, W) = \sum_{m=1}^M b_m (W - W_c)^m$, where we have set $M = 2$ and $N = 2$. For $W < W_c$ we are in the diffusive side and for $W > W_c$ we have localization. Within this approach, F_n , b_m , ν , and W_c are free parameters that we determine using a least-square fit of the gathered data for Λ at sufficiently long times.

We plot in Fig. 2 the numerical points (dots) and the fitted curves (colored lines) from which we obtain the estimates $W_c = 5.94 \pm 0.005$ and $\nu = 2.73 \pm 0.04$, in good agreement with the values $W_c = 5.95$ and $\nu = 2.73$ already reported [37]. Possible corrections due to irrelevant scaling variables [48] can be neglected since the shortest distance over which the spin is randomized is the lattice spacing [37]. In Fig. 3, we plot $\Lambda(t)$ against t for different disorder strengths W . The insulating and metallic regimes are clearly distinguished by their different CBS contrast temporal behaviors and the critical regime is identified by the change in concavity of these time functions. We note that our numerical results are well fitted by the scaling function Eq. (5). At large enough times, according to Eqs. (3) and (4) and the definition of L_t , we expect $\Lambda(t)$ to be essentially constant in the metallic regime and to decay like $1/\sqrt{t}$ in the insulating regime. This constant behavior is indeed observed in the metallic regime for W close enough to the critical disorder W_c . For smaller W we have numerically checked the plateaus for longer times than those shown in the figure. Interestingly, the system still exhibits a residual diffusive motion at the critical point.

This observation is consistent with Wegner's law [49], $s = (d - 2)\nu$, which implies a vanishing critical exponent $s = 0$ for $D \sim (W_c - W)^s$ in two dimensions and thus a constant diffusion coefficient. This behavior has also been observed

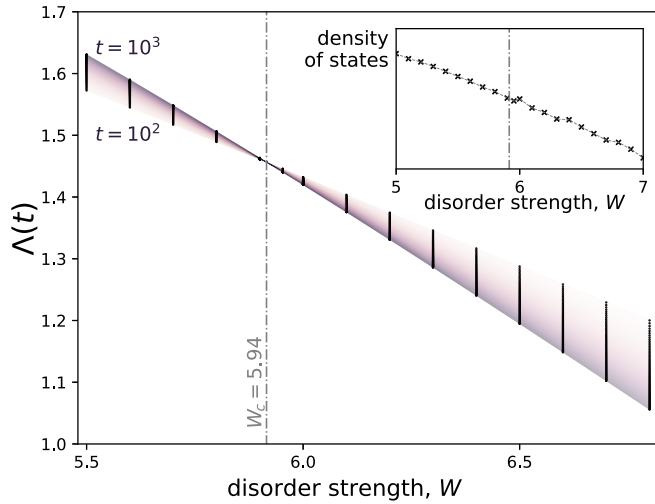


FIG. 2. Inverse scaled CBS width $\Lambda(t)$ for times ranging from $t = 10^2$ to $t = 10^3$ (in units of \hbar/J), as functions of the disorder strength W (in units of J). The longer times correspond to darker curves. The energy is fixed at $E = 1$ (in units of J). All curves cross at the mobility edge $W_c = 5.94 \pm 0.005$ with critical exponent $\nu = 2.73 \pm 0.04$. These values have been extracted from fitting the Taylor expansion of $F(z)$ to the numerical data. The inset shows the smooth behavior of the disorder-average DOS per unit surface area, $\rho(E, W)$, across the transition at energy $E = 1$.

in [50]. To verify the validity of the one-parameter scaling hypothesis in this system, we have numerically extracted $\xi(E, W) = |\eta(E, W)|^{-\nu}$ to collapse all data for $\Lambda(t)$, obtained at different W and times, in Figs. 2 and 3, on a single scaling curve [37].

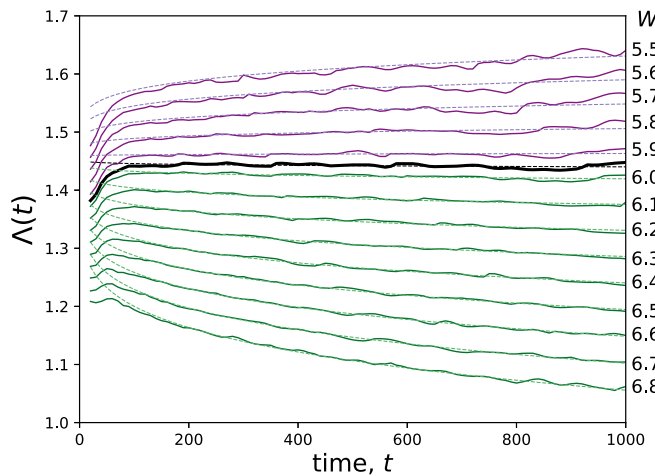


FIG. 3. Solid lines: inverse rescaled CBS width $\Lambda(t)$ as a function of t for different values of the disorder strength W at fixed energy $E = 1$ (in units of J). Curves falling within the metallic and insulator regimes are plotted with blue and green colors, respectively. The thick solid black line corresponds to $W_c = 5.94 \pm 0.005$ and critical exponent $\nu = 2.73 \pm 0.04$. At long times (not shown) $\Lambda(t)$ displays plateaus for $W < W_c$, whereas for $W > W_c$, $\Lambda(t)$ behaves like $1/\sqrt{t}$. Colored dashed lines: fits obtained using the Taylor expansion of the one-parameter scaling function $F(z)$, plotted as a function of t .

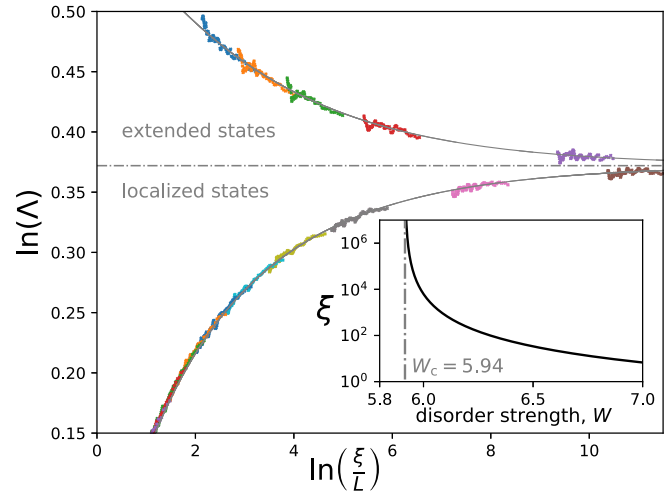


FIG. 4. Scaling function $\ln \Lambda$ as a function of $\ln(\xi/L_t)$ at energy $E = 1$ (in units of J). The different colored pieces on the scaling curve correspond to the data obtained at different W (in units of J). The dashed lines are the fitted curves based on the one-parameter scaling hypothesis; see text. The horizontal gray dash-dotted line marks the separation between the extended and localized branches of the scaling function. The inset shows the correlation length ξ calculated from the CBS width Δk using the numerically extracted parameters $W_c = 5.94 \pm 0.005$ and $\nu = 2.73 \pm 0.04$.

To construct the scaling function, in Fig. 4 $\ln \Lambda(t)$ is plotted as a function of $\ln(1/L_t)$ for different disorder strength W and then shifted horizontally by some quantity $\ln \xi(E, W)$ to construct a smooth continuous curve [51] when $\ln \Lambda(t)$ is plotted as a function of $\ln(\xi/L_t)$. The correlation length ξ , central to the one-parameter scaling hypothesis, identifies with the localization length ξ_{loc} in the insulating phase.

Spin localization. Finally (not shown here), we have observed a spin localization phenomenon in the deep localized regime that we will address in a future work. In this regime, the CBS and CFS peaks become very wide. By broadening, the tails of the CBS dip decrease the background in the spin-flipping channel, while the tails of the CFS peak do the opposite in the spin-preserving channel leading to an imbalanced spin population in the spin channels. Thus the system tends to retain its initial spin state in the deeply localized regime.

Discussion. We have analyzed Anderson localization in an archetypical symplectic system, which is realized in a physical system if spin-orbit coupling is relevant. We have extracted the critical exponent and the critical disorder strength using a finite-time scaling analysis of the coherent backscattering antipeak. The choice of a Gaussian symplectic ensemble confirms the universality of the critical exponent in the symplectic symmetry class. Such an analysis of this momentum-space signature of the phase transition is also accessible in experiment through time-of-flight expansion and absorption imaging.

Furthermore, we have demonstrated that, because the CBS width scales as $t^{-1/2}$ at the transition, there is a residual diffusion in this region in contrast to three-dimensional systems

with a metal-insulator transition. This residual diffusion is a characteristic of any 2D system in which a metal-insulator transition is observed.

A convenient platform to realize our system would be cold atom experiments where Raman transitions are used to produce a 2D spin-orbit effect in an optical lattice [52] or in the bulk [53]. To induce random rotations between lattice sites, we propose to use Raman speckle beams. The on-site disorder can be easily produced by shining another speckle beam onto the atoms [54]. In addition, many results presented here remain true if the hopping terms U_{ij} are not fully random; e.g., if U_{ij} is replaced by $T_{ij} = \alpha \mathbb{1} + (1 - \alpha)U_{ij}$ with $\alpha \in [0, 1]$, then the coefficient α simply controls the area of

the metallic phase in the energy-disorder plane. Future work will study the Anderson transition by monitoring the CFS contrast. However, early computations revealed an additional difficulty in the localized phase: both CBS and CFS peaks exhibit slowly decaying tails in momentum space, leading to an imbalance between the two backgrounds and making an accurate measurement of the CFS contrast troublesome. We are investigating whether this imbalance is solely due to these tails or if it is a signature of AL in the spin degrees of freedom.

Acknowledgments. The Authors acknowledge discussions with Drs John Helm and Jean Decamp useful to the establishment of this project. C.M. would like to thank Keith Slevin for useful discussions.

-
- [1] P. W. Anderson, Absence of diffusion in certain random lattices, *Phys. Rev.* **109**, 1492 (1958).
- [2] M. Cutler and N. F. Mott, Observation of anderson localization in an electron gas, *Phys. Rev.* **181**, 1336 (1969).
- [3] P. A. Lee and T. V. Ramakrishnan, Disordered electronic systems, *Rev. Mod. Phys.* **57**, 287 (1985).
- [4] R. L. Weaver, Anderson localization of ultrasound, *Wave Motion* **12**, 129 (1990).
- [5] R. Dalichaouch, J. P. Armstrong, S. Schultz, P. M. Platzman, and S. L. McCall, Microwave localization by two-dimensional random scattering, *Nature (London)* **354**, 53 (1991).
- [6] D. S. Wiersma, P. Bartolini, A. Lagendijk, and R. Righini, Localization of light in a disordered medium, *Nature (London)* **390**, 671 (1997).
- [7] M. Stoytchev and A. Z. Genack, Microwave transmission through a periodic three-dimensional metal-wire network containing random scatterers, *Phys. Rev. B* **55**, 8617(R) (1997).
- [8] C. Dembowski, H.-D. Gräf, R. Hofferbert, H. Rehfeld, A. Richter, and T. Weiland, Anderson localization in a string of microwave cavities, *Phys. Rev. E* **60**, 3942 (1999).
- [9] M. Störzer, P. Gross, C. M. Aegerter, and G. Maret, Observation of the critical regime near Anderson localization of light, *Phys. Rev. Lett.* **96**, 063904 (2006).
- [10] J. Topolancik, B. Ilic, and F. Vollmer, Experimental observation of strong photon localization in disordered photonic crystal waveguides, *Phys. Rev. Lett.* **99**, 253901 (2007).
- [11] T. Schwartz, G. Bartal, S. Fishman, and M. Segev, Transport and Anderson localization in disordered two-dimensional photonic lattices, *Nature (London)* **446**, 52 (2007).
- [12] H. Hu, A. Strybulevych, J. H. Page, S. E. Skipetrov, and B. A. van Tiggelen, Localization of ultrasound in a three-dimensional elastic network, *Nat. Phys.* **4**, 945 (2008).
- [13] J. Chabé, G. Lemarié, B. Grémaud, D. Delande, P. Szriftgiser, and J. C. Garreau, Experimental observation of the Anderson metal-insulator transition with atomic matter waves, *Phys. Rev. Lett.* **101**, 255702 (2008).
- [14] F. Riboli, P. Barthelemy, S. Vignolini, F. Intonti, A. D. Rossi, S. Combric, and D. S. Wiersma, Anderson localization of near-visible light in two dimensions, *Opt. Lett.* **36**, 127 (2011).
- [15] T. Sperling, W. Bührer, C. M. Aegerter, and G. Maret, Direct determination of the transition to localization of light in three dimensions, *Nat. Photon.* **7**, 48 (2013).
- [16] M. Lopez, J.-F. Clément, P. Szriftgiser, J. C. Garreau, and D. Delande, Experimental test of universality of the anderson transition, *Phys. Rev. Lett.* **108**, 095701 (2012).
- [17] I. Manai, J.-F. Clément, R. Chicireanu, C. Hainaut, J. C. Garreau, P. Szriftgiser, and D. Delande, Experimental observation of two-dimensional anderson localization with the atomic kicked rotor, *Phys. Rev. Lett.* **115**, 240603 (2015).
- [18] T. Ying, Y. Gu, X. Chen, X. Wang, S. Jin, L. Zhao, W. Zhang, and X. Chen, Anderson localization of electrons in single crystals: $\text{Li}_x\text{Fe}_7\text{Se}_8$, *Sci. Adv.* **2**, e1501283 (2016).
- [19] F. Jendrzejewski, K. Müller, J. Richard, A. Date, T. Plisson, P. Bouyer, A. Aspect, and V. Josse, Coherent backscattering of ultracold atoms, *Phys. Rev. Lett.* **109**, 195302 (2012).
- [20] G. Roati, C. D’Errico, L. Fallani, M. Fattori, C. Fort, M. Zaccanti, G. Modugno, M. Modugno, and M. Inguscio, Anderson localization of a non-interacting Bose–Einstein condensate, *Nature (London)* **453**, 895 (2008).
- [21] S. S. Kondov, W. R. McGehee, J. J. Zirbel, and B. DeMarco, Three-dimensional Anderson localization of ultracold matter, *Science* **334**, 66 (2011).
- [22] G. Lemarié, H. Lignier, D. Delande, P. Szriftgiser, and J. C. Garreau, Critical state of the Anderson transition: Between a metal and an insulator, *Phys. Rev. Lett.* **105**, 090601 (2010).
- [23] J. Billy, V. Josse, Z. Zuo, A. Bernard, B. Hambrecht, P. Lugan, D. Clément, L. Sanchez-Palencia, P. Bouyer, and A. Aspect, Direct observation of Anderson localization of matter waves in a controlled disorder, *Nature (London)* **453**, 891 (2008).
- [24] G. Semeghini, M. Landini, P. Castilho, S. Roy, G. Spagnolli, A. Trenkwalder, M. Fattori, M. Inguscio, and G. Modugno, Measurement of the mobility edge for 3D Anderson localization, *Nat. Phys.* **11**, 554 (2015).
- [25] K. Slevin and T. Ohtsuki, Critical exponent for the Anderson transition in the three-dimensional orthogonal universality class, *New J. Phys.* **16**, 015012 (2014).
- [26] Y. Ueoka and K. Slevin, Borel-Dyson symmetry classes, *J. Phys. Soc. Jpn.* **86**, 094707 (2017).
- [27] F. Evers and A. D. Mirlin, Anderson transitions, *Rev. Mod. Phys.* **80**, 1355 (2008).
- [28] C. A. Müller and D. Delande, Disorder and interference: Localization phenomena, in *Ultracold Gases and Quantum Information: Lecture Notes of the Les Houches Summer School in Singapore: Volume 91, July 2009*, edited by C. Miniatura (Oxford University Press, Oxford, 2011), pp. 441–533.

- [29] T. Karpiuk, N. Cherroret, K. L. Lee, B. Grémaud, C. A. Müller, and C. Miniatura, Coherent forward scattering peak induced by anderson localization, *Phys. Rev. Lett.* **109**, 190601 (2012).
- [30] N. Cherroret, T. Karpiuk, C. A. Müller, B. Grémaud, and C. Miniatura, Coherent backscattering of ultracold matter waves: Momentum space signatures, *Phys. Rev. A* **85**, 011604(R) (2012).
- [31] S. Ghosh, N. Cherroret, B. Grémaud, C. Miniatura, and D. Delande, Coherent forward scattering in two-dimensional disordered systems, *Phys. Rev. A* **90**, 063602 (2014).
- [32] S. Ghosh, D. Delande, C. Miniatura, and N. Cherroret, Coherent backscattering reveals the Anderson transition, *Phys. Rev. Lett.* **115**, 200602 (2015).
- [33] D. Thouless, Electrons in disordered systems and the theory of localization, *Phys. Rep.* **13**, 93 (1974).
- [34] E. Abrahams, P. W. Anderson, D. C. Licciardello, and T. V. Ramakrishnan, Scaling theory of localization: Absence of quantum diffusion in two dimensions, *Phys. Rev. Lett.* **42**, 673 (1979).
- [35] N. Mott, The mobility edge since 1967, *J. Phys. C: Solid State Phys.* **20**, 3075 (1987).
- [36] Y. Asada, K. Slevin, and T. Ohtsuki, Anderson transition in the three dimensional symplectic universality class, *J. Phys. Soc. Jpn.* **74**, 238 (2005).
- [37] Y. Asada, K. Slevin, and T. Ohtsuki, Anderson transition in two-dimensional systems with spin-orbit coupling, *Phys. Rev. Lett.* **89**, 256601 (2002).
- [38] G. Orso, Anderson transition of cold atoms with synthetic spin-orbit coupling in two-dimensional speckle potentials, *Phys. Rev. Lett.* **118**, 105301 (2017).
- [39] For spin- $\frac{1}{2}$ system $T = -i\sigma_y K$, where σ_y is the y -Pauli matrix and K the complex conjugation operator. Therefore, $T^2 = -\mathbb{1}$.
- [40] S. Ghosh, Momentum signatures of the Anderson transition, Ph.D. thesis, Centre for Quantum Technologies/National University of Singapore, 2017.
- [41] M. Martinez, G. Lemarié, B. Georgeot, C. Miniatura, and O. Giraud, Coherent forward scattering as a robust probe of multifractality in critical disordered media, *SciPost Phys.* **14**, 057 (2023).
- [42] S. Ghosh, C. Miniatura, N. Cherroret, and D. Delande, Coherent forward scattering as a signature of Anderson metal-insulator transitions, *Phys. Rev. A* **95**, 041602(R) (2017).
- [43] K. L. Lee, B. Grémaud, and C. Miniatura, Dynamics of localized waves in one-dimensional random potentials: Statistical theory of the coherent forward scattering peak, *Phys. Rev. A* **90**, 043605 (2014).
- [44] Y. M. Beltukov and S. E. Skipetrov, Finite-time scaling at the Anderson transition for vibrations in solids, *Phys. Rev. B* **96**, 174209 (2017).
- [45] G. Lemarié, J. Chabé, P. Szriftgiser, J. C. Garreau, B. Grémaud, and D. Delande, Observation of the Anderson metal-insulator transition with atomic matter waves: Theory and experiment, *Phys. Rev. A* **80**, 043626 (2009).
- [46] G. Lemarié, B. Grémaud, and D. Delande, Universality of the Anderson transition with the quasiperiodic kicked rotor, *Europhys. Lett.* **87**, 37007 (2009).
- [47] Y. Asada, K. Slevin, and T. Ohtsuki, The Anderson transition due to random spin-orbit coupling in 2D, *Phys. E* **18**, 274 (2003).
- [48] K. Slevin and T. Ohtsuki, Corrections to scaling at the Anderson transition, *Phys. Rev. Lett.* **82**, 382 (1999).
- [49] F. J. Wegner, Electrons in disordered systems. Scaling near the mobility edge, *Z. Phys. B: Condens. Matter Quanta* **25**, 327 (1976).
- [50] T. Kawarabayashi and T. Ohtsuki, Diffusion of electrons in two-dimensional disordered symplectic systems, *Phys. Rev. B* **53**, 6975 (1996).
- [51] Y. Asada, K. Slevin, and T. Ohtsuki, Numerical estimation of the β function in two-dimensional systems with spin-orbit coupling, *Phys. Rev. B* **70**, 035115 (2004).
- [52] Z. Wu, L. Zhang, W. Sun, X.-T. Xu, B.-Z. Wang, S.-C. Ji, Y. Deng, S. Chen, X.-J. Liu, and J.-W. Pan, Realization of two-dimensional spin-orbit coupling for Bose-Einstein condensates, *Science* **354**, 83 (2016).
- [53] L. Huang, Z. Meng, P. Wang, P. Peng, S.-L. Zhang, L. Chen, D. Li, Q. Zhou, and J. Zhang, Experimental realization of two-dimensional synthetic spin-orbit coupling in ultracold Fermi gases, *Nat. Phys.* **12**, 540 (2016).
- [54] F. Jendrzejewski, A. Bernard, K. Müller, P. Cheinet, V. Josse, M. Piraud, L. Pezzé, L. Sanchez-Palencia, A. Aspect, and P. Bouyer, Three-dimensional localization of ultracold atoms in an optical disordered potential, *Nat. Phys.* **8**, 398 (2012).